Boosting subdominant neutralizing antibody responses with a computationally designed epitope-focused immunogen

Authors:

Sesterhenn F[1,2], Galloux M[3], Vollers SS[1], Csepregi L[4], Yang C[1,2], Descamps D[3], Bonet J[1,2], Friedensohn S[4], Gainza P[1,2], Corthésy P[1], Chen M[5], Rosset S[1], Rameix-Welti MA[6,7], Eléouët JF[3], Reddy ST[4], Graham BS[5], Riffault S[3] & Correia BE[1,2,*].

Affiliations:

[1] Institute of Bioengineering, École Polytechnique Fédérale de Lausanne, Lausanne CH-1015, Switzerland.
[2] Swiss Institute of Bioinformatics (SIB), Lausanne CH-1015, Switzerland.
[3] Unité de Virologie et Immunologie Moléculaires (UR892), INRA, Université Paris-Saclay, 78352, Jouy-en-Josas, France.
[4] Department of Biosystems Science and Engineering, ETH Zurich, Basel, Switzerland.
[5] Viral Pathogenesis Laboratory, Vaccine Research Center, National Institute of Allergy and Infectious Diseases, National Institutes of Health, Bethesda, MD, United States.
[6] UMR1173, INSERM, Université de Versailles St. Quentin, 78180 Montigny le Bretonneux, France.
[7] AP-HP, Laboratoire de Microbiologie, Hôpital Ambroise Paré, 92104, Boulogne-Billancourt, France.
[*] Corresponding author: bruno.correia@epfl.ch

Abstract

Throughout the last decades, vaccination has been key to prevent and eradicate infectious diseases. However, many pathogens (e.g. respiratory syncytial virus (RSV), influenza, dengue and others) have resisted vaccine development efforts, largely due to the failure to induce potent antibody responses targeting conserved epitopes. Deep profiling of human B-cells often reveals potent neutralizing antibodies that emerge from natural infection, but these specificities are generally subdominant (i.e., are present in low titers). A major challenge for next-generation vaccines is to overcome established immunodominance hierarchies and focus antibody responses on crucial neutralization epitopes. Here, we show that a computationally designed epitope-focused immunogen presenting a single RSV neutralization epitope elicits superior epitope-specific responses compared to the viral fusion protein. In addition, the epitope-focused immunogen efficiently boosts antibodies targeting the Palivizumab epitope, resulting in enhanced neutralization. Overall, we show that epitope-focused immunogens can boost subdominant neutralizing antibody responses *in vivo* and reshape established antibody hierarchies.

Introduction

The development of vaccines has proven to be one of the most successful medical interventions to reduce the burden of infectious diseases (*1*), and their correlate of protection is the induction of neutralizing antibodies (nAbs) that block infection (*2*).

In recent years, advances in high-throughput B-cell technologies have revealed a plethora of potent nAbs for different pathogens which have resisted the traditional means of vaccine development for several decades, including HIV-1 (*3*), influenza (*4*), respiratory syncytial virus (RSV) (*5, 6*), zika (*7, 8*), dengue (*9*) and others (*10-12*). A major target of these nAb responses is the pathogens fusion protein, which drives the viral and host cell membrane fusion while undergoing a conformational rearrangement from a prefusion to a postfusion state (*13*). Many of these nAbs have been structurally characterized in complex with their target, unveiling the atomic details of neutralization epitopes (*7, 14, 15*). Together, these studies have provided comprehensive antigenic maps of the viral fusion proteins which delineate epitopes susceptible to antibody-mediated neutralization and provide a roadmap for rational and structure-based vaccine design approaches.

The conceptual framework to leverage neutralizing antibody-defined epitopes for vaccine development is commonly referred to as reverse vaccinology (*16, 17*). Although reverse vaccinology-inspired approaches have yielded a number of exciting advances in the last decade, the design of immunogens that elicit such focused antibody responses remains challenging. Successful examples of structure-based immunogen design approaches include conformational stabilization of RSVF in its prefusion state, which induces superior serum neutralization titers when compared to immunization with F in the postfusion conformation (*18*). In the case of influenza, several epitopes targeted by broadly neutralizing antibodies (bnAbs) were identified within the hemagglutinin (HA) stem domain, and an HA stem-only immunogen elicited a broader neutralizing antibody response than full-length HA (*19, 20*). Commonly, these approaches have aimed to focus antibody responses on specific conformations or subdomains of viral proteins. In a more aggressive approach, Correia et al. (*21*) computationally designed a synthetic immunogen presenting the RSV antigenic site II (Figure 1a), and provided a proof-of-principle for the induction of site specific, RSV neutralizing antibodies using a synthetic immunogen.

The absence of a potent and long-lasting immune response upon natural infection is a major challenge associated with RSV, influenza virus and other pathogens. While single exposure to pathogens like poliovirus confers life-long immunity, RSV, influenza and other pathogens have developed mechanisms to subvert the development of a durable and potent neutralizing antibody response, thereby allowing such pathogens to infect humans repeatedly throughout their lives (*22*). One of the major factors hindering the induction of long-lasting protection after the first infection is related to the antibody specificities induced. Upon exposure to a pathogen, such as influenza, the human antibody responses predominantly target strain-specific antigenic sites, whereas potent bnAbs are subdominant (*23*). This phenomenon is generally referred to as B-cell immunodominance, which describes the unbalanced immunogenicity of certain antigenic sites within an antigen, favoring strain-specific, variable, non-neutralizing epitopes to the detriment of conserved, neutralization-sensitive epitopes (*24*). The factors that determine the antigenicity of specific epitopes remain unclear, making the categorization of immunodominant and subdominant epitopes an empirical classification based on serological analysis. Importantly, the presence of high levels of antibodies directed against immunodominant epitopes can sterically mask surrounding subdominant epitopes that may be targeted by bnAbs, preventing the immune system from mounting productive antibody responses against subdominant epitopes, and potentially limiting vaccination efficacy (*23-26*).

The immunodominance hierarchy is established within the germinal center, where B-cells undergo a binding affinity-based competition for available antigen and subsequently initiate a clonal expansion stage, ultimately becoming long-lived plasma cells or memory B-cells (*27*). Controlling this competition and driving antibody responses towards the increased recognition of subdominant, neutralizing epitopes is of primary importance to enable development of novel vaccines to fight pathogens which have resisted traditional strategies. One of the few strategies to guide antibody maturation was tested in the HIV field and is referred to as germline targeting, which relies upon the activation and expansion of rare but specific B-cell lineages in naïve individuals (*28, 29*). In contrast, under conditions of pre-existing immunity acquired during natural infection or previous vaccination, the challenge is to manipulate already established B-cell immunodominance hierarchies and reshape serum antibody

107 responses towards desired specificities. In an indirect approach towards increasing
108 subdominant B-cell populations, Silva et al. (*30*) have shown that the targeted
109 suppression of immunodominant clones during an active germinal center reaction can
110 allow subdominant B-cell populations to overtake the germinal center response. Other
111 approaches have used heterologous prime-boost immunization regimens with either
112 alternative viral strains or rationally modified versions of the priming immunogen (*31-*
113 *34*) in order to steer antibody responses towards more conserved domains. However,
114 leveraging structural information of defined neutralization epitopes to guide bulk
115 antibody responses towards specific, well-characterized single epitopes remains an
116 unmet challenge.
117
118 Here, we investigate whether, under conditions of pre-existing immunity, a
119 computationally designed immunogen presenting a single epitope is able to reshape
120 serum antibody responses towards increased recognition of a specific neutralizing
121 epitope. To mimic a scenario of pre-existing immunity against a relevant pathogen, we
122 immunized mice with a prefusion-stabilized version of RSVF, and found that antibody
123 titers against RSV antigenic site II were present in very low levels, i.e. a subdominant
124 epitope-specific response was elicited. Based on a previously developed epitope-
125 focused immunogen for RSV site II (FFL_001) (*21*), we engineered an optimized
126 nanoparticle presenting this immunogen, and investigated the potential of a rationally
127 designed epitope-focused immunogen to boost these subdominant levels of site-
128 specific antibodies.
129 We show that multivalent presentation of a designed epitope-focused immunogen
130 elicits superior levels of epitope-specific antibodies compared to prefusion RSVF in
131 naïve mice, indicating that the subdominance of a particular epitope can be altered
132 through its presentation in a distinct molecular context. Repeated immunizations with
133 RSVF failed to increase site II-specific antibodies, and instead further diluted site II
134 specific responses. In contrast, heterologous boosts with an epitope-scaffold
135 nanoparticle enhanced serum responses towards the subdominant site
136 II epitope, and the boosted antibodies neutralized RSV *in vitro*. For the first time, we
137 provide compelling evidence that synthetic immunogens comprising a single epitope
138 can efficiently redirect specificities in bulk antibody responses *in vivo* and enhance
139 subdominant neutralizing antibody responses. Such strategy may present an

important alternative for pathogens where future vaccines are required to reshape pre-existing immunity and elicit finely tuned antibody specificities.

142 **Results**

143

144 Design of an RSV-based nanoparticle displaying a site II epitope-focused immunogen

145 In a previous study, a computationally-designed, RSV site II epitope-scaffold
146 nanoparticle was shown to elicit serum neutralization activity in non-human primates
147 (NHPs) (*21*). Despite the fact that very potent monoclonal antibodies were isolated
148 from the immunized NHPs, the neutralization potency at serum level was modest,
149 indicating low titers of the potent antibodies. Therefore, our first aim was to take the
150 best previously tested immunogen (FFL_001) and further optimize the immunogen
151 delivery and immunization conditions to maximize the induction of site II-specific
152 antibodies. A comparative study of four different adjuvants revealed that Alhydrogel®,
153 an adjuvant approved for human use, yielded highest overall immunogenicity and
154 elicited antibodies cross-reactive with prefusion RSVF in four out of five mice
155 (Supplementary Fig. 1).

156

157 Next, we sought to develop an improved, easily produced nanoparticle to multimerize
158 the epitope-scaffold for efficient B-cell receptor crosslinking. Previously, Correia et al.
159 (*21*) employed a chemical conjugation strategy of FFL_001 to a Hepatitis-B core
160 antigen based nanoparticle, which resulted in a difficult construct with a laborious
161 purification process. Recently, several studies have reported the use of RSV
162 nucleoprotein (RSVN) as a nanoparticle platform for immunogen presentation (*35, 36*).
163 When expressed in *E. coli*, RSVN forms nanorings, 17 nm in diameter, containing 10
164 or 11 RSVN protomers (*37*). We reasoned that RSVN would be an ideal particle
165 platform to multimerize an RSV epitope-scaffold, as RSVN contains strong, RSV-
166 directed T-cell epitopes (*36*). However, our initial attempts to genetically fuse FFL_001
167 to RSVN yielded poorly soluble proteins that rapidly aggregated after purification. We
168 therefore employed structure-based protein resurfacing (*38*), attempting to improve
169 the solubility of this site II epitope-scaffold when arrayed in high density on RSVN. To
170 guide our resurfacing design process, we leveraged information from a sequence
171 homolog of the ribosomal recycling factor (PDB: 1ISE), the structural template
172 originally used to design FFL_001. Based on a sequence alignment of the mouse
173 homolog (NCBI reference: NP_080698.1) and FFL_001, we exchanged the FFL_001
174 amino acids for the mouse sequence homolog and used Rosetta Fixed Backbone
175 Design (*39*) to ensure that the mutations were not energetically unfavorable, resulting

176 in 38 amino acid substitutions (34.2% overall). We named this variant FFLM, whose
177 expression yields in *E. coli* showed a five-fold increase when compared to FFL_001,
178 and it was confirmed to be monomeric in solution (Supplementary Fig. 2).
179
180 To confirm that the resurfacing did not alter the epitope integrity, we measured the
181 binding affinities of FFLM to Motavizumab, a high-affinity variant of Palivizumab (*40*),
182 and to a panel of human site II nAbs previously isolated (*5*) using surface plasmon
183 resonance (SPR). All antibodies bound with high affinity to FFLM, indicating broad
184 reactivity of this immunogen with a diverse panel of human nAbs (Figure 1b).
185 Interestingly, the tested nAbs showed approximately one order of magnitude higher
186 affinity to the epitope-scaffold as compared to the latest version of prefusion RSVF,
187 originally called DS2 (*41*), suggesting that the epitope is properly presented and likely
188 further stabilized in a relevant conformation.
189
190 Importantly, the FFLM-RSVN fusion protein expressed with high yields in *E. coli* (>10
191 mg/liter), forming a nanoring particle, dubbed NRM, that was monodisperse in solution
192 with a diameter of approximately 21 nm (Figure 1c). Although we cannot fully
193 rationalize the factors that contributed to the solubility improvement upon
194 multimerization, our strategy to transplant surface residues from a sequence homolog
195 to synthetic proteins may prove useful to enhance the solubility of other
196 computationally designed proteins.
197

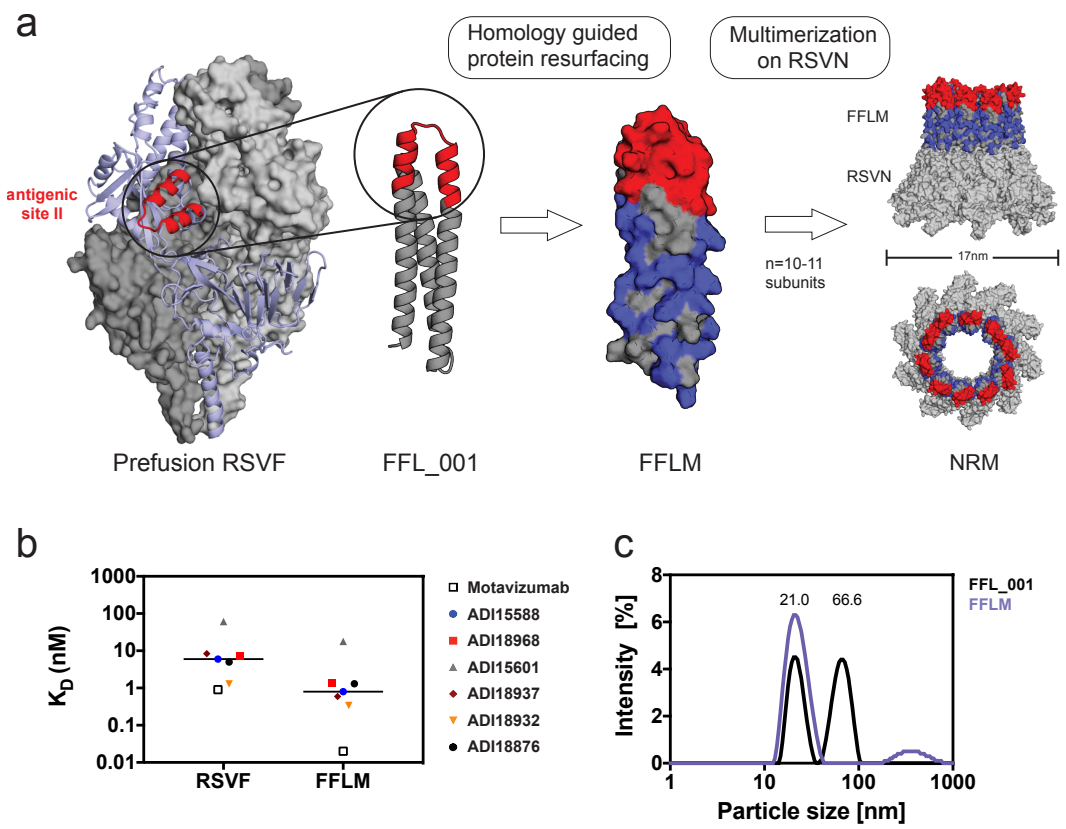

Figure 1:

Design of an RSV-based nanoparticle displaying a site II epitope-focused immunogen. a) Structural model of the prefusion RSVF trimer (PDBID: 4JHW), with two subunits shown as a grey surface and one subunit shown as light blue cartoon representation with the epitope targeted by Palivizumab (antigenic site II) highlighted in red. FFL_001 was previously designed to present the site II epitope in a computationally designed scaffold. FFLM was designed by evolution-guided resurfacing, where changes in amino acid identity are highlighted in blue. FFLM was genetically fused to the N-terminus of the RSV nucleoprotein (RSVN), resulting in a high-density array of the epitope-scaffold, as shown by the structural model (based on PDBID: 2WJ8). **b)** Binding affinities of site II-specific human nAbs measured by SPR. K_Ds were measured with RSVF/FFLM immobilized as ligand and antibody fabs as analyte. nM = nanomolar. **c)** Dynamic light scattering (DLS) profiles for FFL_001 and FFLM fused to RSVN. The FFL_001-RSVN fusion protein formed higher-order oligomers in solution (66.6 nm of median diameter), whereas the resurfaced FFLM-

215 RSVN fusion protein (NRM) was monodisperse with a median diameter of 21 nm. nm
216 = nanometer.
217
218 NRM enhances the induction of site II-specific antibodies
219 We next tested the immunogenicity of the site II scaffold nanoring and its ability to elicit
220 site II-specific antibodies. Three groups of ten mice were subjected to three
221 immunizations with 10 μg of NRM, monomeric FFLM and prefusion RSVF (*41*), which
222 is currently the leading immunogen for an RSV vaccine (Figure 2a). Based on the
223 results of our adjuvant screen (Supplementary Fig. 1), all the immunogens were
224 formulated in Alhydrogel, an adjuvant approved for human use. As compared to FFLM,
225 NRM showed a higher overall immunogenicity (directed both against RSVN and
226 FFLM) (Figure 2b).
227
228 A key aspect of epitope-focused vaccines is to understand how much of the antibody
229 response targets the viral epitope presented to the immune system. Therefore, we
230 sought to measure the site II-specific antibody titers elicited by NRM and FFLM and
231 compare these epitope-specific antibody responses to those elicited by prefusion
232 RSVF. Using an SPR competition assay to measure site II-specific antibodies in sera
233 (described in methods), we observed that NRM elicited site II-specific antibody
234 responses superior to those elicited by RSVF (Figure 2c). This was surprising, given
235 that the ratio of site II epitope surface area to overall immunogen surface is similar in
236 both NRM and RSVF (Supplementary Fig. 2). To confirm this finding through a direct
237 binding assay rather than a competitive format, we measured the binding levels of
238 sera to the site II epitope in a peptide ELISA, where the site II peptide was immobilized
239 on a streptavidin-coated surface. Consistent with the previous experiment, we found
240 that NRM elicited two orders of magnitude higher site II-specific responses than RSVF
241 (Figure 2d). Together, we concluded that an epitope-focused immunogen, despite
242 similar molecular surface area, can elicit substantially higher levels of site-specific
243 antibodies compared to a viral fusion protein.

Fig. 2

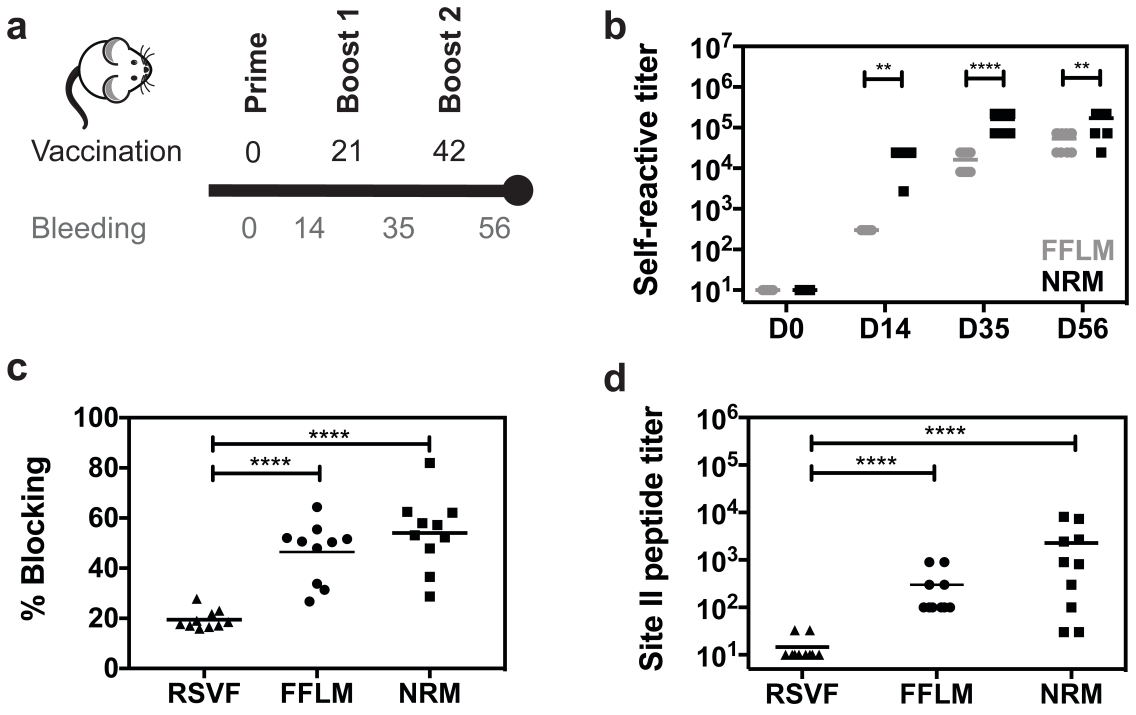

Figure 2:
Immunogenicity and quantification of site II-specific antibody responses. a) Immunization scheme. Balb/c mice were immunized three times on days 0, 21 and 42, and blood was drawn 14 days after each vaccination. **b)** Serum antibody titers elicited by FFLM and NRM at different timepoints measured by ELISA against the respective immunogen. NRM shows significantly increased immunogenicity at day 14, 35 and 56 relative to FFLM. **c)** SPR competition assay with Motavizumab. Day 56 sera of mice immunized with RSVF, FFLM or NRM was diluted 1:100 and SPR response units (RU) were measured on sensor chip surfaces containing the respective immunogen. Motavizumab binding sites were then blocked by saturating amounts of Motavizumab, and the residual serum response was measured to calculate the serum fraction competed by Motavizumab binding. Mice immunized with FFLM or NRM show significantly higher levels of serum antibodies that are competed by Motavizumab binding. **d)** Site II-specific serum titers at day 56 from mice immunized with RSVF, FFLM and NRM, measured by ELISA against site II peptide. Three immunizations with prefusion RSVF elicited low levels of site II-specific antibodies, whereas FFLM and NRM vaccinations yielded significantly higher peptide-specific serum titers. Data shown are derived from at least two independent experiments, each sample assayed

264 in duplicate. Statistical comparisons were calculated using two-tailed Mann-Whitney
265 U tests. ** indicates $p < 0.01$, *** indicates $p < 0.0001$, **** $p < 0.0001$.

266 NRM induces low levels of RSVF cross-reactive antibodies with low neutralization
267 potency

268 Given the substantial site II-specific serum titers elicited by NRM in mice, we
269 investigated whether these antibodies cross-reacted with prefusion RSVF and were
270 sufficient to neutralize RSV *in vitro*.

271

272 Following three immunizations with NRM, all the mice (n=10) developed detectable
273 serum cross-reactivity with prefusion RSVF (mean serum titer = 980) (Figure 3a).
274 Unsurprisingly, the overall quantity of prefusion RSVF cross-reactive antibodies
275 elicited by immunization with an immunogen presenting a single epitope is more than
276 two orders of magnitude lower than those of mice immunized with prefusion RSVF,
277 which comprises at least six antigenic sites (*5*). Similarly, a B-cell ELISpot revealed
278 that NRM-immunized mice presented prefusion RSVF-reactive antibody secreting
279 cells, but their frequency was approximately one order of magnitude lower than upon
280 immunization with prefusion RSVF (Figure 3c).

281

282 The major determinant for antibody specificity is attributed to the heavy chain CDR3
283 region (HCDR3) (*42*). While for certain classes of nAbs, the antibody lineages and
284 their sequence features are well-defined (e.g. HIV neutralizing VRC01 class
285 antibodies (*43*), or RSV neutralizing MPE8-like antibodies (*44*)), antibodies targeting
286 RSV antigenic site II seem to be derived from diverse precursors and do not show
287 HCDR3 sequence convergence in humans (*5*). While we did not expect to find
288 dominant lineages or HCDR3 sequence patterns in mice, we used next-generation
289 antibody repertoire sequencing (*45*) to ask whether NRM could elicit antibodies with
290 similar sequence signatures to those elicited by prefusion RSVF. Indeed, we found
291 300 clonotypes, defined as antibodies derived from the same VH gene with the same
292 HCDR3 length and 80% sequence similarity, that overlapped between NRM and the
293 prefusion RSVF immunized cohort, suggesting that at the molecular level, relevant
294 antibody lineages can be activated with the NRM immunogen (Supplementary Figure
295 3). Notably, nine out of the 20 most expanded clonotypes in the NRM cohort were also
296 present in mice immunized with prefusion RSVF, albeit not as expanded (Figure 3b).

297 This finding might reflect the enrichment of site II specific antibodies in the NRM cohort
298 (Figure 2d).
299 We further investigated whether these low levels of prefusion RSVF-binding
300 antibodies were sufficient to neutralize RSV *in vitro*. While three immunizations with
301 prefusion RSVF elicited potent RSV-neutralizing serum titers (mean IC_{50}= 10,827), for
302 NRM we only detected low levels of RSV-neutralizing serum activity in three out of ten
303 mice (Figure 3d). This result is consistent with Correia *et al*. (*21*), who observed no
304 serum neutralization in mice, but succeeded in inducing nAbs in NHPs with prior RSV
305 seronegativity.
306
307 Altogether, we concluded that despite NRM's superior potential to induce high levels
308 of site II-specific antibodies, the majority of antibodies activated from the naïve
309 repertoire is not functional for RSV neutralization. A potential explanation, stemming
310 from structural comparison between the epitope-focused immunogen (FFLM) and
311 RSVF, is that although epitope-specific antibodies are abundantly elicited by NRM,
312 these antibodies do not recognize the site II epitope in its native RSVF quaternary
313 environment in the prefusion conformation, or on virions in sufficient amounts and with
314 high enough affinity to potently neutralize RSV.

Fig. 3

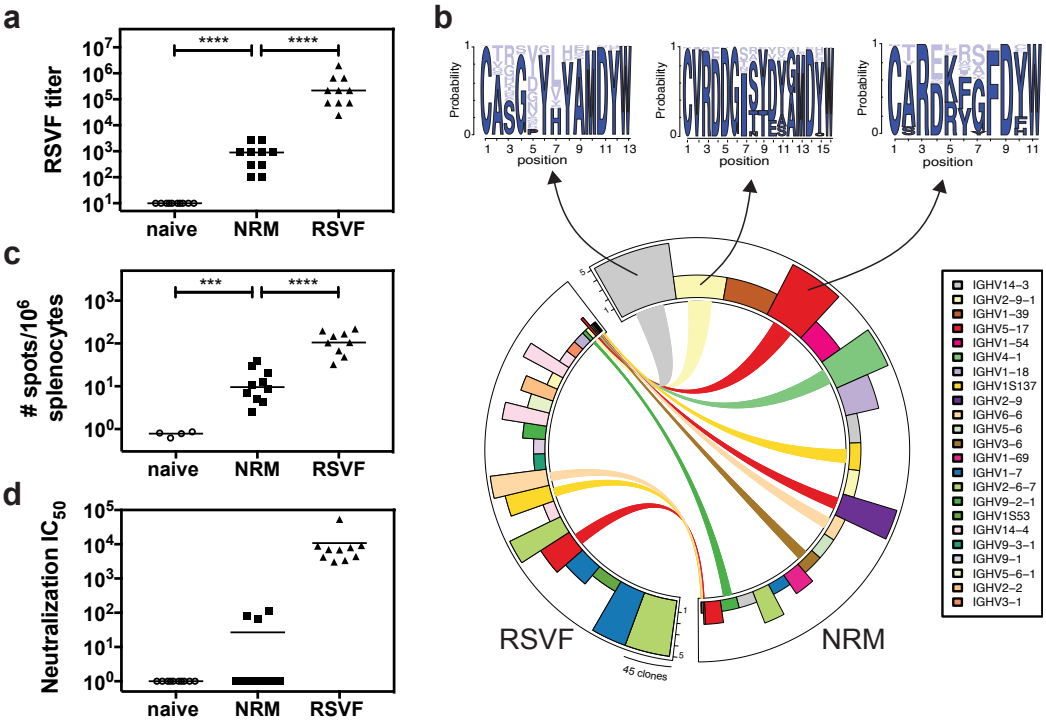

Figure 3:

RSVF cross-reactivity and serum neutralization. **a)** NRM elicits prefusion RSVF cross-reactive antibodies, which are two orders of magnitude lower compared to prefusion RSVF immunization. Mice immunized only with adjuvant (naïve) do not show RSVF cross-reactivity. **b)** Next-generation sequencing of antibody repertoire. Antibody variable heavy chains of mice immunized with RSVF or NRM (5 mice per cohort) were sequenced and grouped into clonotypes. Circos plot showing the 20 most expanded clonotypes from both cohorts, with identical clonotypes connected. Height of bars indicates number of mice that showed the respective clonotype, width represents the clonal expansion within a clonotype (i.e. the number of clones grouped into the respective clonotype). Three clonotypes that occurred both in the RSVF and the NRM cohort, but were expanded within the NRM cohort were analyzed for their HCDR3 sequence profile, as shown by sequence logo plots (top). Dark blue color represents amino acid identities that occurred in RSVF cohort, light blue color represents amino acids uniquely found following NRM immunization. The frequency of each amino acid in the NRM cohort is indicated by the size of the letter. **c)** B-cell ELISpot of mouse splenocytes to quantify prefusion RSVF-specific antibody secreting cells (ASC).

334 Number of ASCs per 10^6 splenocytes that secrete prefusion RSVF-specific antibodies
335 following three immunizations with adjuvant only (naïve), NRM or prefusion RSVF **d)**
336 RSV neutralizing activity of mouse sera from day 56 shown as neutralization IC_{50}.
337 Three out of ten mice immunized with NRM showed detectable RSV neutralizing
338 activity, whereas all mice immunized with prefusion RSVF neutralized RSV (mean IC_{50}
339 = 10,827). Data shown are from one out of two independent experiments. Statistical
340 comparisons were calculated using two-tailed Mann-Whitney U tests. *** indicates $p <$
341 0.001, **** indicates $p < 0.0001$.

342 NRM boosts site II-specific antibodies under conditions of pre-existing immunity
343 While vaccination studies in naïve animal models are an important first step to validate
344 novel immunogens, previous studies (*21*) and results presented here imply that
345 epitope-scaffolds may not be able to elicit robust RSV neutralizing serum activity from
346 a naïve antibody repertoire. However, given the high affinity of the epitope-scaffold
347 towards a panel of site II- specific nAbs, together with the ability to elicit high titers of
348 site II-specific antibodies *in vivo*, we hypothesized that such an epitope focused
349 immunogen could be efficient in recalling site II-specific B-cells in a scenario of pre-
350 existing immunity, thereby achieving an enhanced site-specific neutralization
351 response.
352
353 Our initial immunization studies with prefusion RSVF showed that site II-specific
354 responses were subdominant (Figure 2c and 2d). Given that subdominance is a
355 common immunological phenotype for many of the neutralization epitopes that are
356 relevant for vaccine development (*46*), we sought to test if NRM could boost
357 subdominant antibody lineages that should ultimately be functional and recognize the
358 epitope in the tertiary environment of the viral protein. To test this hypothesis, we
359 designed a mouse immunization experiment with three cohorts, as outlined in Figure
360 4a. Following a priming immunization with RSVF, cohort (1) was boosted with adjuvant
361 only ("prime only"), cohort (2) received two boosting immunizations with prefusion
362 RSVF ("homologous boost"), and cohort (3) received two boosts with NRM
363 ("heterologous boost").
364
365 A comparison between prefusion RSVF immunized groups prime only and
366 homologous boost revealed that the two additional boosting immunizations with RSVF
367 only slightly increased overall titers of prefusion RSVF-specific antibodies ($p = 0.02$),
368 indicating that a single immunization with adjuvanted RSVF is sufficient to induce close
369 to maximal serum titers against RSVF (Figure 4b). Following the heterologous boost
370 with NRM, overall RSVF specific antibody titers remained statistically comparable to
371 the prime only group ($p = 0.22$).
372
373 Next, we quantified the site II-specific endpoint serum titers in a peptide ELISA format
374 (Figure 4c). Interestingly, the homologous boost with prefusion RSVF failed to
375 increase site II-specific antibody levels, reducing the responses directed to site II to

376 the lower limit of detection by ELISA. This result is yet another example of the
377 underlying complexity inherent to the fine specificity of antibody responses elicited by
378 immunogens and how important specificities can be dampened throughout the
379 development of an antibody response. In contrast to the homologous boost, the
380 heterologous boost with NRM significantly increased site II peptide-specific serum
381 titers ($p < 0.0001$).
382
383 In order to understand whether this increase relied at least partially on an actual recall
384 of antibodies primed by RSVF, or rather on an independent antibody response
385 irrelevant for RSVF binding and RSV neutralization, we dissected the epitope
386 specificity within the RSVF-specific serum response. In an SPR competition assay, a
387 significantly higher fraction ($p = 0.02$) of prefusion RSVF-reactive antibodies were
388 competed by Motavizumab in mouse sera primed with prefusion RSVF and boosted
389 with NRM (mean % competition = 37.5 ± 14.5%), as compared to mice immunized
390 once or three times with prefusion RSVF (21.5% ± 12.1% or 19.5% ± 3.7%,
391 respectively) (Figure 4d). Similarly, a competition ELISA revealed that a significantly
392 larger fraction of overall RSVF reactivity was attributed to site II-specific antibodies
393 upon heterologous boost, as compared to both control groups (36.1% ± 2.5% versus
394 22.6% ± 9.1% or 14.4% ±5.9%, respectively, $p = 0.002$ and $p < 0.0001$). In contrast,
395 site II-specific antibodies were significantly higher in mice that received only one as
396 opposed to three RSVF immunizations, indicating that RSVF boosting immunizations
397 further diluted site II-specific antibody titers ($p = 0.03$) (Figure 4e).
398
399 Together, we have shown that the serum antibody specificity can be steered towards
400 a well-defined antigenic site by boosting pre-existing, subdominant antibody levels
401 with an epitope focused immunogen. This is an important and distinctive feature of the
402 epitope focused immunogen compared to an immunogen based on a viral protein
403 (prefusion RSVF), which was shown to decrease already subdominant antibody
404 responses under the same conditions. These results may have broad implications on
405 strategies to control antibody fine specificities in vaccination schemes, both for RSV
406 and other pathogens.

Fig. 4

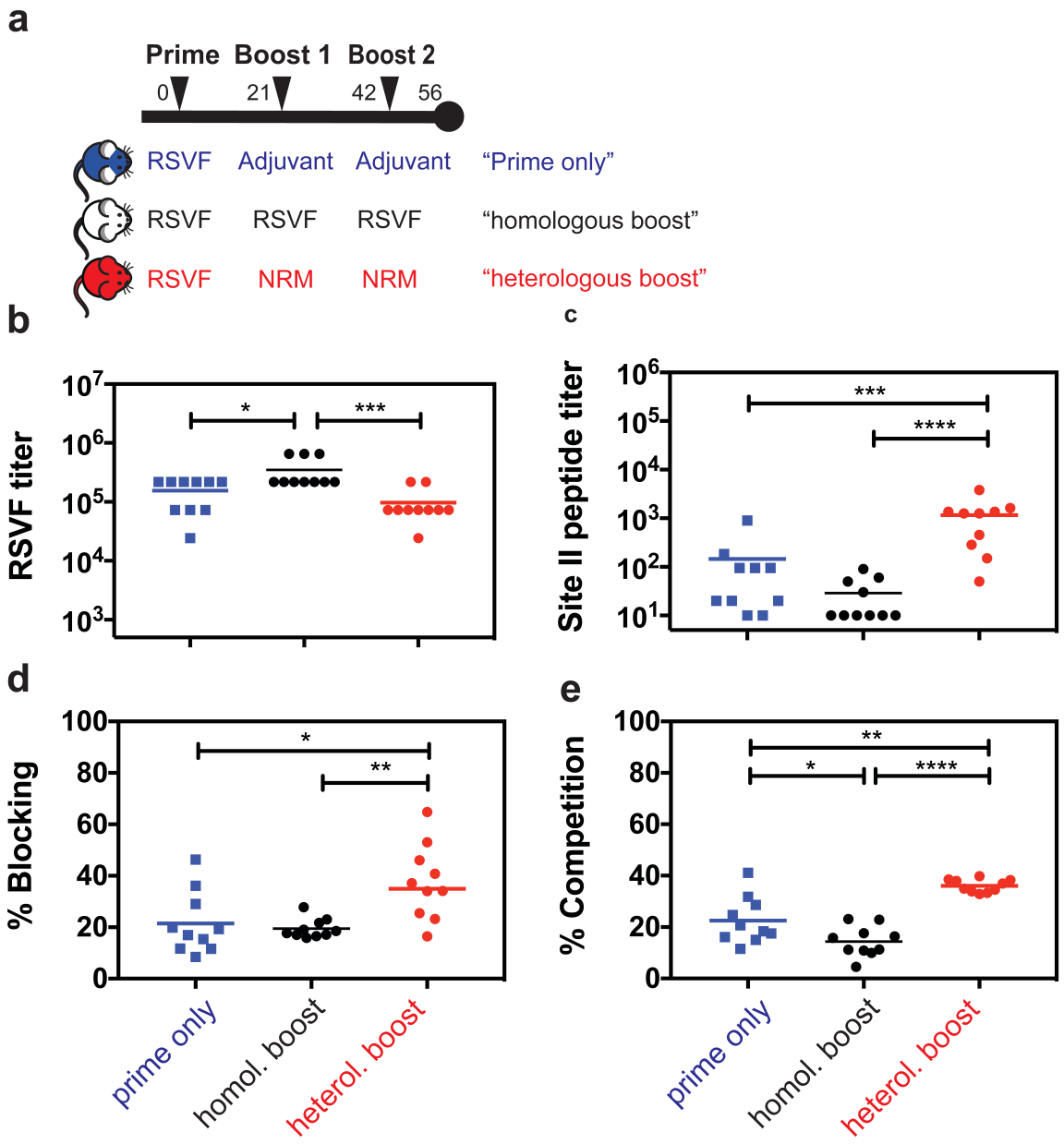

Figure 4:

Heterologous prime boost reshapes antibody responses enhancing levels of site II specific antibodies. a) Heterologous prime-boost study groups. Three mouse cohorts were immunized with either 1x RSVF ("prime only"), 3x RSVF ("homologous boost") or 1x RSVF followed by two boosts with NRM ("heterologous boost"). **b)** Antibody titers directed against prefusion RSVF. Mice receiving homologous boosting immunizations show slightly higher RSVF-specific serum titers compared to the prime only cohort, whereas heterologous boosting yielded statistically comparable titers to the prime only group. The difference between the homologous and heterologous boost

417 cohorts was statistically significant. **c)** Site II-specific titers measured by ELISA
418 showed that the heterologous boost significantly increases site II-specific titers
419 compared to both prime and homologous boost groups. Albeit not statistically
420 significant ($p = 0.06$), mice receiving a homologous boost had lower levels of site II-
421 specific antibodies compared to prime only group. **d)** SPR competition assay with
422 Motavizumab on a prefusion RSVF-coated sensor chip. Sera from indicated groups
423 were diluted 1:100 and RSVF binding responses were quantified. Site II was then
424 blocked with Motavizumab, and the remaining serum response quantified. The
425 heterologous boost induced a significantly higher fraction of site II-directed antibodies
426 competed with Motavizumab for RSVF binding, as compared to both prime only and
427 homologous boost groups). **e)** Quantification of site II-specific responses in a
428 competition ELISA. Binding was measured against prefusion RSVF, and the Area
429 Under the Curve (AUC) was calculated in presence of NRM competitor, normalized to
430 the AUC in the presence of RSVN as a control competitor. Compared to the prime
431 only group, the homologous boost resulted in significantly lower site II-specific serum
432 titers, confirming the trend observed in c). The heterologous boost increased the
433 fraction of site II-targeting antibodies within the pool of prefusion RSVF-specific
434 antibodies compared to both control groups. Data presented are from at least two
435 independent experiments, with each sample assayed in duplicates. Statistical
436 comparisons were calculated using two-tailed Mann-Whitney U tests. * indicates
437 $p<0.05$, ** indicates $p < 0.01$, *** indicates $p < 0.0001$, **** $p < 0.0001$.

438 Boosted antibodies neutralize RSV *in vitro*

439 The enhanced reactivity to site II observed in the heterologous prime-boost scheme
440 led us to investigate if antibodies boosted by a synthetic immunogen were functionally
441 relevant for virus neutralization. In bulk sera, we observed 2.3-fold higher serum
442 neutralization titers in mice receiving a heterologous boost (mean IC_{50}=7,654)
443 compared to the prime only control group (mean IC_{50}=3,275) (Figure 5a). While this
444 increase in serum neutralization was not statistically significant, we next assessed if
445 this increase in neutralization was driven by increased levels of epitope-specific
446 antibodies. We observed that site II-directed antibody levels correlated with overall
447 serum neutralization titers in the heterologous prime boost group (r^2=0.76, p=0.0009)
448 (Figure 5b), whereas prime only (r^2=0.32, p=0.09) or animals receiving a homologous
449 boost showed no such correlation (r^2 = 0.18, p=0.22) (Supplementary Figure 4). To
450 characterize the neutralizing serum activity dependence on antigenic site II, we pooled
451 mouse sera within each cohort, enriched site II-specific antibodies and measured viral
452 neutralization (see methods). Briefly, we incubated pooled sera from each group with
453 streptavidin beads conjugated to biotin-labeled antigenic site II peptide, and eluted
454 bound antibodies. To control for the quality of the enrichment protocol, we verified by
455 ELISA that the column flow-through was depleted of site II-specific antibodies
456 (Supplementary Figure 5).

457

458 Strikingly, mice receiving a heterologous boost showed a 15-fold increase in site II-
459 mediated neutralization as compared to mice immunized once or three times with
460 prefusion RSVF (Figure 5c). We performed the same experiment for mice immunized
461 three times with NRM and did not detect any RSV neutralization in this format. This
462 observation is consistent with the very low levels of bulk sera neutralization measured
463 in this group, indicating that NRM can only boost nAbs under conditions of pre-existing
464 immunity. In summary, we conclude that the heterologous boosting scheme with a
465 single epitope immunogen enhanced subdominant neutralizing antibody responses
466 directed against the antigenic site presented, and effectively redirected an antibody
467 response *in vivo*.

468

469

Fig. 5

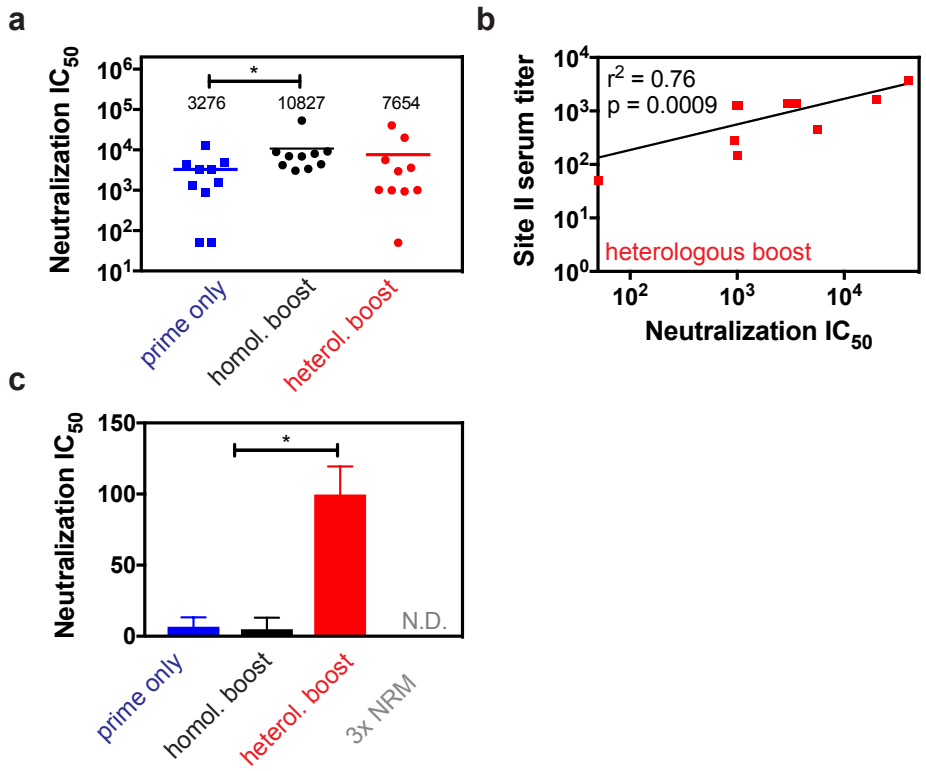

470
471 Figure 5

472 **Boosted site II-specific antibodies are functional and mediate increased**
473 **neutralization activity. a)** *In vitro* RSV neutralization IC_{50} for each group. Compared
474 to the prime only group, mice receiving a homologous boost showed increased RSV
475 neutralization titers. On average, the heterologous boost yielded a 2.3-fold increase in
476 serum neutralization titers compared to prime only, but these differences were
477 statistically not significant when compared to either group. **b)** Correlation of site II-
478 specific serum titer (measured by peptide ELISA) with RSV neutralization IC_{50} as
479 determined for each mouse within the heterologous prime boost cohort. Correlations
480 for control groups are shown in Supplementary Figure 4. Data represent the mean of
481 two independent experiments, each measured in duplicate. Pearson correlation
482 coefficient (r^2) and p-value were calculated in GraphPad Prism. **c)** Site II-specific
483 antibody fractionation revealed increased levels of nAbs. Site II-specific antibodies
484 from mouse sera were enriched in an affinity purification. Those isolated from the
485 heterologous boost group showed a 15-fold increase in RSV neutralizing activity
486 compared to both control groups. No site II-mediated neutralization was detected for
487 mice receiving three immunizations of NRM (N.D. = non-detectable). Data are

488 presented from two independent experiments, and each sample was assayed in
489 duplicate with additional controls shown in Supplementary Figure 5. Statistical
490 comparisons were calculated using two-tailed Mann-Whitney U tests. * indicates $p <$
491 0.05.

492 **Discussion**

493

494 Despite a rapid increase in our atomic-level understanding of antibody-antigen
495 interactions for various pathogens, the translation of structural information into
496 efficacious immunogens that elicit antibody responses specific to *bona fide* epitopes
497 remains a key challenge for next-generation vaccine development.

498

499 Multiple strategies have been investigated to focus nAb responses on defined
500 neutralization epitopes (*47*). Among them, epitope-scaffolds have been shown to elicit
501 RSV site II-specific, neutralizing antibody responses in naïve non-human primates.
502 While the overall serum neutralization was modest, a monoclonal antibody induced by
503 vaccination, showed superior neutralization potency to that of Palivizumab (*21*).
504 However, a major limitation of epitope-scaffold immunogens (*48-50*) is that the
505 quaternary environment of the epitope presented in the native viral protein is lost.
506 Thus, the binding mode of a significant fraction of the elicited antibodies is likely
507 incompatible with the epitope in its native environment. This observation is reinforced
508 by our finding that although NRM elicited high serum levels of site II-directed
509 antibodies, only residual neutralizing activity was observed in mice, which is consistent
510 with previous studies using epitope-scaffolds (*50-52*). Together, these results highlight
511 the limitations of synthetic scaffolds in an epitope-focused vaccine approach in naïve
512 individuals.

513

514 However, our finding that a subdominant epitope (site II) in its native environment
515 (prefusion RSVF) is readily targeted by the immune system when presented in a
516 distinct molecular context (NRM), supported the potential use of synthetic
517 immunogens to reshape antibody responses towards *bona fide* vaccine epitopes. Pre-
518 existing immunity against a viral protein (RSVF, influenza HA or others), in which
519 certain antibody specificities are subdominant, is a common scenario in humans that
520 have encountered repeated natural infections throughout their life (*26, 53-55*).
521 Therefore, a major challenge for vaccine development is to boost pre-existing,
522 subdominant antibodies to enhance site-specific neutralization.

523

524 To date, boosting nAbs targeting specific epitopes under conditions of pre-existing
525 immunity has been challenging. For instance, strong antibody responses against

526 immunodominant epitopes can sterically mask the neutralization epitope, preventing
527 the induction of a potent antibody response targeting the subdominant site (*23, 25, 26,*
528 *56*). Overcoming these established immunodominance hierarchies is complex, as
529 such hierarchies seem to be impacted by multiple factors including serological
530 antibody levels, their specificity, memory B-cell counts, adjuvants, and the
531 immunization or infection route (*24*).
532
533 Heterologous prime-boost schemes are a promising strategy to guide the fine
534 specificity of antibody responses and to focus these responses on vulnerable antigenic
535 sites. Several vaccine studies have been conducted for influenza (*33, 34*), RSV (*31*)
536 and HIV (*28*), where the heterologous immunogens were alternative strains or
537 modified viral fusion proteins, but yet not as heterologous as a computationally
538 designed epitope-scaffold. An important point to consider regarding immunogens
539 based on modified viral proteins is whether immunodominant signatures remain,
540 steering the antibody responses away from the target epitopes. While this scenario
541 may not be fully absent in synthetic epitope-scaffolds, it is at least mitigated by the fact
542 that the protein has not evolved under the pressure of escaping the immune system.
543
544 Our study demonstrates that a heterologous boosting immunogen with a single
545 neutralization epitope, when optimally presented can enhance pre-existing,
546 subdominant antibody responses targeting this epitope. The ability to narrowly focus
547 antibody responses to a single epitope that mediates clinical protection, underlines the
548 potential of rationally designed immunogens for vaccine development against elusive
549 pathogens. In particular, our results demonstrate that albeit single-epitope
550 immunogens may not be the most powerful to select functional antibodies from a naïve
551 repertoire, they have a unique ability to boost neutralizing epitope-specific antibodies
552 primed by a viral protein. Further studies in more relevant animal models will reveal if
553 neutralizing antibodies primed by natural infection with RSV can also be boosted
554 mimicking a more realistic vaccination scenario.
555
556 Given that the approach presented here is generalizable and that epitope-scaffold
557 nanoparticles can be proven successful in boosting nAbs specific for other sites, this
558 strategy holds great potential to tune levels of antibody specificities through

559 heterologous prime boost vaccination schemes which are now frequently used in for
560 challenging pathogens (*28, 33, 57*).
561
562 The original antigenic sin theory in the influenza field describes that the first viral
563 exposure permanently shapes the antibody response, which causes individuals to
564 respond to seasonal vaccines dependent on their immune history (*23, 58*). Seasonal
565 vaccines generally fail to boost antibodies targeting broadly neutralization epitopes on
566 the hemagglutinin stem region (*23*). Focusing antibody responses on these defined
567 epitopes may remove the need for annual vaccine reformulation, and may also protect
568 against emerging pandemic strains (*14, 46, 59, 60*). The influenza vaccine challenge
569 seems particularly well suited to our approach considering that the human population
570 has pre-existing immunity to influenza, including some subdominant bnAbs that
571 seasonal vaccines fail to stimulate (*23*).
572 Lastly, vaccine development against antigenically related viruses such as zika and
573 dengue could benefit of the approach presented here, as antibodies mounted against
574 the envelope protein of a dengue subtype can facilitate infection with zika (*61*) or other
575 dengue subtypes (*62*). A site conserved between all four dengue subtypes and zika
576 envelope protein has been structurally characterized and suggested for the
577 development of an epitope-focused immunogen (*7*).
578
579 When seeking to apply an immunofocusing strategy to other antigenic sites and
580 pathogens, one challenge is the development of epitope-scaffolds stably presenting
581 the epitope in a synthetic immunogen that is compatible with antibody binding. While
582 the RSV antigenic site II is a structurally simple helix-turn-helix motif, many other
583 identified neutralization epitopes comprise multiple, discontinuous segments.
584 However, continuous advances in rational protein design techniques (*63*) will allow the
585 design of more complex protein scaffolds to stabilize increasingly complex epitopes.
586
587 Altogether, we have shown how an optimized presentation of a computationally
588 designed immunogen in an RSVN-based nanoparticle can reshape bulk serum
589 responses and boost subdominant, neutralizing antibody responses *in vivo.* This is a
590 distinctive feature compared to using prefusion RSVF as a boosting immunogen, and
591 underscores how subdominant epitopes can be converted to immunodominant
592 epitopes when presented in a different environment. We foresee the great promise of

593 this strategy to overcome the challenge of boosting and focusing pre-existing immunity
594 towards defined neutralization epitopes, potentially applicable to multiple pathogens.

Methods

Resurfacing

The previously published RSV site II epitope-scaffold ("FFL_001") (*21*) was designed based on a crystal structure of a mutant of ribosome recycling factor from *E. coli* (PDB entry 1ISE. Using BLAST, we identified sequence homologs of 1ISE from eukaryotic organisms and created a multiple sequence alignment with clustal omega (CLUSTALO (1.2.1)) (*64*) of the mouse homolog sequence (NCBI reference NP_080698.1), 1ISE and FFL_001. Surface-exposed residues of FFL_001 were then mutated to the respective residue of the mouse homolog using the Rosetta fixed backbone design application (*39*), resulting in 38 surface mutations. Amino acid changes were verified to not impact overall Rosetta energy score term.

Protein expression and purification

FFLM

DNA sequences of the epitope-scaffold designs were purchased from Genscript and cloned in pET29b, in frame with a C-terminal 6x His tag. The plasmid was transformed in *E. coli* BL21 (DE3) and grown in Terrific Broth supplemented with Kanamycin (50 µg/ml). Cultures were inoculated to an OD_{600} of 0.1 from an overnight culture and incubated at 37°C. After reaching OD_{600} of 0.6, expression was induced by the addition of 1 mM isopropyl-β-D-thiogalactoside (IPTG) and cells were incubated for further 4-5h at 37°C. Cell pellets were resuspended in lysis buffer (50 mM TRIS, pH 7.5, 500 mM NaCl, 5% Glycerol, 1 mg/ml lysozyme, 1 mM PMSF, 1 µg/ml DNase) and sonicated on ice for a total of 12 minutes, in intervals of 15 seconds sonication followed by a 45 seconds pause. Lysates were clarified by centrifugation (18,000 rpm, 20 minutes), sterile-filtered and purified using a His-Trap FF column on an Äkta pure system (GE healthcare). Bound proteins were eluted in buffer containing 50 mM Tris, 500 mM NaCl and 300 mM imidazole, pH 7.5. Concentrated proteins were further purified by size exclusion chromatography on a Superdex™ 75 300/10 (GE Healthcare) in PBS. Protein concentrations were determined via measuring the absorbance at 280 nm on a Nanodrop (Thermo Scientific). Proteins were concentrated

628 by centrifugation (Millipore, #UFC900324) to 1 mg/ml, snap frozen in liquid nitrogen
629 and stored at -80°C.
630
631 NRM
632 The full-length N gene (sequence derived from the human RSV strain Long, ATCC
633 VR-26; GenBank accession number AY911262.1) was PCR amplified using the
634 Phusion DNA polymerase (Thermo Scientific) and cloned into pET28a+ at NcoI-XhoI
635 sites to obtain the pET-N plasmid. The sequence of FFLM was then PCR amplified
636 and cloned into pET-N at NcoI site to the pET-NRM plasmid. *E. coli* BL21 (DE3)
637 bacteria were co-transformed with pGEX-PCT (*65*) and pET-FFLM-N plasmids and
638 grown in LB medium containing ampicillin (100 µg/ml) and kanamycin (50 µg/ml). The
639 same volume of LB medium was then added, and protein expression was induced by
640 the addition of 0.33 mM IPTG to the medium. Bacteria were incubated for 15 h at 28°C
641 and then harvested by centrifugation. For protein purification, bacterial pellets were
642 resuspended in lysis buffer (50 mM Tris-HCl pH 7.8, 60 mM NaCl, 1 mM EDTA, 2 mM
643 dithiothreitol, 0.2% Triton X-100, 1 mg/ml lysozyme) supplemented with a complete
644 protease inhibitor cocktail (Roche), incubated for one hour on ice, and disrupted by
645 sonication. The soluble fraction was collected by centrifugation at 4 °C for 30 min at
646 10,000 x g. Glutathione-Sepharose 4B beads (GE Healthcare) were added to clarify
647 supernatants and incubated at 4°C for 15h. The beads were then washed one time in
648 lysis buffer and two times in 20 mM Tris pH 8.5, 150 mM NaCl. To isolate NRM, beads
649 containing bound complex were incubated with thrombine for 16 h at 20 °C. After
650 cleavage of the GST tag, the supernantant was loaded onto a Sephacryl S-200 HR
651 16/30 column (GE Healthcare) and eluted in 20 mM Tris-HCl, 150 mM NaCl, pH 8.5.
652
653 Antibody variable fragments (Fabs)
654 For Fab expression, heavy and light chain DNA sequences were purchased from Twist
655 Biosciences and cloned separately into the pHLSec mammalian expression vector
656 (Addgene, #99845) using AgeI and XhoI restriction sites. Expression plasmids were
657 pre-mixed in a 1:1 stoichiometric ratio, co-transfected into HEK293-F cells and
658 cultured in FreeStyle™ medium (Gibco, #12338018). Supernatants were harvested
659 after one week by centrifugation and purified using a kappa-select column (GE
660 Healthcare). Elution of bound proteins was conducted using 0.1 M glycine buffer (pH

661 2.7) and eluates were immediately neutralized by the addition of 1 M Tris ethylamine
662 (pH 9), followed by buffer exchange to PBS pH 7.4.
663
664 Respiratory Syncytial Virus Fusion protein (prefusion RSVF)
665 Protein sequence of prefusion RSVF corresponds to the sc9-10 DS-Cav1 A149C
666 Y458C S46G E92D S215P K465Q variant designed by Joyce et al. (*41*), which we
667 refer to as RSVF DS2. RSVF DS2 was codon optimized for mammalian expression
668 and cloned into the pHCMV-1 vector together with two C-terminal Strep-Tag II and
669 one 8x His tag. Plasmids were transfected in HEK293-F cells and cultured in
670 FreeStyle™ medium. Supernatants were harvested one week after transfection and
671 purified via Ni-NTA affinity chromatography. Bound protein was eluted using buffer
672 containing 10 mM Tris, 500 mM NaCl and 300 mM Imidazole (pH 7.5), and eluate was
673 further purified on a StrepTrap HP affinity column (GE Healthcare). Bound protein was
674 eluted in 10mM Tris, 150 mM NaCl and 20 mM Desthiobiotin (Sigma), pH 8, and size
675 excluded in PBS, pH 7.4, on a Superdex 200 Increase 10/300 GL column (GE
676 Healthcare) to obtain trimeric RSVF.
677
678 Affinity determination using Surface Plasmon Resonance
679 Surface Plasmon Resonance experiments were performed on a Biacore 8K at room
680 temperature with HBS-EP+ running buffer (10 mM HEPES pH 7.4, 150 mM NaCl, 3
681 mM EDTA, 0.005 % v/v Surfactant P20) (GE Healthcare). Approximately 100
682 response units (RU) of FFLM were immobilized via amine coupling on a CM5 sensor
683 chip (GE Healthcare). Serial dilutions of site II-specific antibody variable fragments
684 (fabs) were injected as analyte at a flow rate of 30 µl/min with 120 seconds contact
685 time. Following each injection cycle, ligand regeneration was performed using 0.1 M
686 glycine, pH 2. Data analysis was performed using 1:1 Langmuir binding kinetic fits
687 within the Biacore evaluation software (GE Healthcare).
688
689 Mouse immunizations
690 All animal experiments were approved by the Veterinary Authority of the Canton of
691 Vaud (Switzerland) according to Swiss regulations of animal welfare (animal protocol
692 number 3074). Six-week-old, female Balb/c mice were ordered from Janvier labs and
693 acclimatized for one week. Immunogens were thawed on ice and diluted in PBS pH
694 7.4 to a concentration of 0.2 mg/ml. The immunogens were then mixed with an equal

695 volume of 2% Alhydrogel® (Invivogen), resulting in a final Alhydrogel concentration
696 of 1%. Other adjuvants were formulated according to manufacturer's instructions.
697 After mixing immunogens and adjuvants for one hour at 4°C, each mouse was
698 injected with 100 μl, corresponding to 10 μg immunogen adsorbed to Alhydrogel. All
699 immunizations were done subcutaneously, with no visible irritation around the
700 injection site. Immunizations were performed on day 0, 21 and 42. 100-200 μl blood
701 were drawn on day 0, 14, 35, and the maximum amount of blood (200-1000μl) was
702 taken by cardiac puncture at day 56, when mice were sacrificed.
703
704 Antigen ELISA
705 Nunc Medisorp plates (Thermo Scientific, # 467320) were coated overnight at 4°C with
706 100 μl of antigen (recombinant RSVF, FFLM and NRM) diluted in coating buffer (100
707 mM sodium bicarbonate, pH 9) at a final concentration of 0.5 μg/ml. For blocking,
708 plates were incubated for two hours at room temperature with blocking buffer (PBS +
709 0.05% Tween 20 (PBST) supplemented with 5% skim milk powder (Sigma, #70166)).
710 Mouse sera were serially diluted in blocking buffer and incubated for one hour at room
711 temperature. Plates were washed five times with PBST before adding 100 μl of anti-
712 mouse HRP-conjugated secondary antibody diluted at 1:1500 in blocking buffer
713 (abcam, #ab99617). An additional five washes were performed before adding Pierce
714 TMB substrate (Thermo Scientific, # 34021). The reaction was stopped by adding 100
715 μl of 2M sulfuric acid, and absorbance at 450 nm was measured on a Tecan Safire 2
716 plate reader.
717 Each plate contained a standard curve of Motavizumab to normalize signals between
718 different plates and experiments. Normalization was done in GraphPad Prism. The
719 mean value was plotted for each cohort and statistical analysis was performed using
720 GraphPad Prism.
721
722 Competition ELISA
723 Prior to incubation with a coated antigen plate, sera were serially diluted in the
724 presence of 100 μg/ml competitor antigen and incubated overnight at 4°C. ELISA
725 curves of a positive control, Motavizumab, are shown in Supplementary Figure 6.
726 Curves were plotted using GraphPad Prism, and the area under the curve (AUC) was

727 calculated for the specific (NRM) and control (RSVN) competitor. % competition was
728 calculated using the following formula (*66*):
729
730 % competition = $(1 - (\frac{AUC(specific\ competitor\ (NRM))}{AUC(control\ competitor\ (NR))})) * 100$
731
732 Peptide sandwich ELISA
733 The antigenic site II was synthesized as peptide by JPT Peptide Technologies,
734 Germany. The following sequence was synthesized and biotinylated at the N-
735 terminus:
736 MLTNSELLSKINDMPITNDQKKLMSNNVQI
737 For ELISA analysis of peptide-reactive serum antibodies, Nunc MediSorp plates were
738 coated with 5 μg/ml streptavidin (Thermo Scientific, #21122) for one hour at 37°C.
739 Subsequently, ELISA plates were blocked as indicated above, followed by the addition
740 of 2.4 μg/ml of the biotinylated site II peptide. Coupling was performed for one hour at
741 room temperature. The subsequent steps were performed as described for the antigen
742 ELISA.
743
744 Serum competition using Surface Plasmon Resonance
745 Approximately 300 RU of antigen were immobilized via amine coupling on a CM5 chip.
746 Mouse sera were diluted 1:100 in HBS-EP+ running buffer and flowed as analyte with
747 a contact time of 120 seconds to obtain an initial response unit ($RU_{non\text{-}blocked\ surface}$).
748 The surface was regenerated using 50 mM NaOH. Sequentially, Motavizumab was
749 injected four times at a concentration of 2 μM, leading to complete blocking of
750 Motavizumab binding sites as confirmed by signal saturation. The same serum dilution
751 was reinjected to determine the remaining response ($RU_{blocked\ surface}$). The delta serum
752 response (ΔSR) corresponds to the baseline-subtracted, maximum signal of the
753 injected sera.
754
755 $$\Delta \mathrm{SR} = \mathrm{RU}_{(\mathrm{non-})\mathrm{blocked\ surface}} - \mathrm{RU}_{\mathrm{Baseline}}$$
756
757 Percent blocking was calculated as follows:
758

759 $$\% \text{ blocking} = (1 - (\frac{\Delta\, SR_{\text{blocked surface}}}{\Delta\, SR_{\text{non-blocked surface}}})) * 100$$

760

761 A schematic representation of the SPR experiment is shown in Supplementary Figure
762 7, and calculated blocking values are shown in Supplementary Table 1.

763

764 Enzyme-linked immunospot assay (ELISPOT)

765 B-cell ELISPOT assays were performed using the Mouse IgG ELISpot HRP kit
766 (Mabtech, #3825-2H) according to the manufacturer's instructions. Briefly, mouse
767 spleens were isolated, and pressed through a cell strainer (Corning, #352350) to
768 obtain a single cell suspension. Splenocytes were resuspended in RPMI media
769 (Gibco, #11875093) supplemented with 10% FBS (Gibco), Penicillin/Streptomycin
770 (Gibco), 0.01 µg/ml IL2, 1 µg/ml R848 (Mabtech, #3825-2H) and 50 µM β-
771 mercaptoethanol (Sigma) for ~60 hours stimulation at 37 °C, 5% CO_2. ELISpot plates
772 (PVDF 96-well plates, Millipore, #MSIPS4510) were coated overnight with 15 µg/ml
773 antigen diluted in PBS, followed by careful washing and blocking using RPMI + 10%
774 FBS. Live splenocytes were counted and the cell number was adjusted to $1x10^7$
775 cells/ml. Serial dilutions of splenocytes were plated in duplicates and incubated
776 overnight with coated plates. After several wash steps with PBS buffer, plates were
777 incubated for two hours with biotinylated anti-mouse total IgG (Mabtech, # 3825-6-
778 250) in PBS, followed by incubation with streptavidin-conjugated to HRP (Mabtech,
779 #3310-9) for one hour. Spots were revealed using tetramethylbenzidine (TMB,
780 Mabtech, #3651-10) and counted with an automatic reader (Bioreader 2000; BioSys
781 GmbH). Results were represented as number of spots per 10^6 splenocytes.

782

783 RSV neutralization assay

784 The RSV A2 strain carrying a luciferase gene (RSV-Luc) was a kind gift of Marie-Anne
785 Rameix-Welti, UFR des Sciences et de la Santé, Paris. Hep2 cells were seeded in
786 Corning 96-well tissue culture plates (Sigma, #CLS3595) at a density of 40,000
787 cells/well in 100 µl of Minimum Essential Medium (MEM, Gibco, #11095-080)
788 supplemented with 10% FBS (Gibco, 10500-084), L-glutamine 2 mM (Gibco, #25030-
789 081) and penicillin-streptomycin (Gibco, #15140-122), and grown overnight at 37 °C
790 with 5% CO2.

791 Sera were heat-inactivated for 30 minutes at 56 °C. Serial two-fold dilutions were
792 prepared in an untreated 96-well plate using MEM without phenol red (M0, Life
793 Technologies, #51200-038) containing 2mM L-glutamine, penicillin + streptomycin,
794 and mixed with 800 pfu/well RSV-Luc (corresponding to a final MOI of 0.01). After
795 incubating diluted sera and virus for one hour at 37 °C, growth media was removed
796 from the Hep2 cell layer and 100 μl/well of the serum-virus mixture added. After 48
797 hours, cells were lysed in 100 µl buffer containing 32 mM Tris pH 7.9, 10 mM $MgCl_2$,
798 1.25% Triton X-100, 18.75% glycerol and 1mM DTT. 50 µl lysate were transferred to
799 a 96-well plate with white background (Sigma, # CLS3912). 50 µl of lysis buffer
800 supplemented with 1 µg/ml luciferin (Sigma, #L-6882) and 2 mM ATP (Sigma, #A3377)
801 were added to each well immediately before reading luminescence signal on a Tecan
802 Infinite 500 plate reader.
803 On each plate, a Palivizumab dilution series was included to ensure comparability of
804 neutralization data. In our assay, we determined IC_{50} values for Palivizumab of 0.32
805 µg/ml, which is similar to what other groups have reported (*40*). The neutralization
806 curve was plotted and fitted using the GraphPad variable slope fitting model, weighted
807 by $1/Y^2$.
808
809 Sera fractionation
810 400 µl of streptavidin agarose beads (Thermo Scientific, #20347) were pelleted at
811 13,000 rpm for 2 minutes in a table top centrifuge and washed with phosphate buffered
812 saline (PBS). 200 µg of biotinylated site II peptide were incubated for 2 hours at room
813 temperature to allow coupling of biotinylated peptide to streptavidin beads. Beads
814 were washed three times with 1 ml PBS to remove excess of peptide and resuspended
815 to a total volume of 500 µl bead slurry. Mouse sera from the same cohort (n=10) were
816 pooled (4 µl each, 40 µl total) in a total volume of 200 µl PBS, and 90 µl diluted sera
817 were mixed with 150 µl of bead slurry, followed by an overnight incubation at 4 °C.
818 Beads were pelleted by centrifugation and the supernatant carefully removed by
819 pipetting. Beads were then washed twice with 200 µl PBS and the wash fractions were
820 discarded. To elute site II-specific antibodies, beads were resuspended in 200 µl
821 elution buffer (0.1 M glycine, pH 2.7) and incubated for 1 minute before centrifugation.
822 Supernatant was removed, neutralized with 40 µl neutralization buffer (1 M Tris pH
823 7.5, 300 mM NaCl), and stored at -20 °C for subsequent testing for RSV neutralization.

824 As a control, unconjugated streptavidin was used for each sample to account for non-
825 specific binding.
826
827 Next-generation antibody repertoire sequencing (NGS)
828 RNA isolation
829 Mouse bone marrow was isolated from femurs and re-suspended in 1.5 ml Trizol (Life
830 Technologies, #15596) and stored at -80˚C until further processing. RNA extraction
831 was performed using the PureLink RNA Mini Kit (Life Technologies, #12183018A)
832 following the manufacturer guidelines.
833
834 Antibody sequencing library preparation
835 Library preparation for antibody variable heavy chain regions was performed using a
836 protocol that incorporates unique molecular identifier (UID) tagging, as previously
837 described in Khan *et al.* (*67*). Briefly, first-strand cDNA synthesis was performed by
838 using Maxima reverse transcriptase (Life Technologies, #EP0742) following the
839 manufacturer instructions, using 5 µg RNA with 20 pmol of IgG gene-specific primers
840 (binding IgG1, IgG2a, IgG2b, IgG2c, and IgG3) with an overhang of a reverse UID
841 (RID). After cDNA synthesis, samples were subjected to a left-hand sided SPRIselect
842 bead (Beckman Coulter, #B23318) cleanup at 0.8X. Quantification of target-specific
843 cDNA by a digital droplet (dd)PCR assay allowed exact input of 135000 copies into
844 the next PCR step. Reaction mixtures contained a forward multiplex primer set that
845 was specific for variable heavy region framework 1 and possessed forward UID (FID),
846 a 3' Illumina adapter specific reverse primer, and 1X KAPA HIFI HotStart Uracil+
847 ReadyMix (KAPA Biosystems, #KK2802). PCR reactions were then left-hand side
848 SPRIselect bead cleaned as before and quantified using ddPCR assay. Finally, an
849 Illumina adaptor-extension PCR step was carried out using 820000 copies of the
850 previous PCR product. Following 2nd-step adaptor-extension PCR, reactions were
851 cleaned using a double-sided SPRIselect bead cleanup process (0.5X-0.8X) and
852 eluted in TE buffer.
853
854 NGS with Illumina MiSeq (2 x 300 bp)
855 After library preparation, individual NGS libraries were characterized for quality and
856 quantified by capillary electrophoresis using a Fragment Analyzer (Advanced
857 Analytical DNF-473 Standard Sensitivity). Samples were then pooled and NGS was

858 performed on the Illumina MiSeq platform with a MiSeq Reagent Kit V3, 2x300bp
859 paired-end (Illumina, #MS-102-3003), using an input concentration of 10 pM with 10%
860 PhiX.
861
862 Error and bias correction
863 Error and bias correction was performed using molecular amplification fingerprinting
864 pipeline, as previously described (*67, 68*).
865 1) Bioinformatic preprocessing
866 Paired-end FASTQ files obtained from Illumina MiSeq were imported into CLC
867 Genomics Workbench 10 on the ETH Zurich Euler High Performance Computing
868 (HPC) cluster. A preprocessing workflow was run containing the following steps:
869 trimming of low quality reads, merging of paired-end reads, removal of sequences not
870 aligning to mouse IGH constant sequences, and length filtering.
871
872 2) Error correction by consensus building
873 After pre-processing all datasets were downsampled to contain the same amount of
874 sequencing reads as the dataset with the lowest overall number of reads (361749
875 sequencing reads). For error correction, a custom Python script was used to perform
876 consensus building on the sequences for which at least three reads per UID were
877 required. VDJ annotation and frequency calculation was then performed by our in-
878 house aligner (*67, 68*). The complete error-correction and alignment pipeline is
879 available under https://gitlab.ethz.ch/reddy/MAF.
880
881 Sequence analysis and data visualization
882 Data analysis was done by customized scripts in R. For the identification of clonotypes
883 hierarchical clustering (*68*) was utilized to group CDR3 sequences together. The
884 following parameters were used: identical IGHV and IGHJ gene segment usage,
885 identical CDR3 length, and at least 80% CDR3 amino acid similarity to one other
886 sequence in the given clonotype (single linkage). The overlap of clonotypes between
887 both cohorts was analyzed by extracting the 20 most expanded clonotypes from each
888 cohort and visualizing their size, occurrence, and Vgene usage by a circos plot using
889 R software circlize (*69*). CDR3 sequence similarities between overlapping clonotypes
890 were represented graphically with the R software motifStack (*70*). All scripts are
891 available upon request.

892

893 **Data availability**

894 Data supporting the findings of this study are available within the article and its
895 Supplementary Information, or are available from the authors upon request.

896 **Contributions**

897 F.S. and B.E.C. designed experiments. M.G. expressed and purified RSVN and NRM
898 fusion protein. F.S., C.Y., S.S.V and P.C performed ELISAs. F.S. designed and
899 performed SPR competition assay. F.S., C.Y and P.C performed ELISpot
900 experiments, S.S.V, P.C and S.R performed mouse immunizations. L.C and S.F
901 performed next generation sequencing analysis. F.S., J.B. and P.G. designed FFLM.
902 F.S., P.C and M.C. performed RSV neutralization assay. F.S. and B.E.C wrote the
903 paper. All authors commented on the manuscript.

904

905 **Acknowledgements**

906 We thank Stefan Kunz for helpful discussions and critical reading of the manuscript.
907 This work was supported by the Swiss initiative for systems biology (SystemsX.ch),
908 the European Research Council (Starting grant - 716058) and the Swiss National
909 Science Foundation.

910

911 **Competing interests**

912 The authors declare no competing financial interests.

913

914 **References**

915 1. R. Rappuoli, C. W. Mandl, S. Black, E. De Gregorio, Vaccines for the twenty-first
916 century society. *Nat Rev Immunol* **11**, 865-872 (2011).
917 2. S. A. Plotkin, Correlates of protection induced by vaccination. *Clin Vaccine Immunol*
918 **17**, 1055-1065 (2010).
919 3. D. R. Burton, L. Hangartner, Broadly Neutralizing Antibodies to HIV and Their Role in
920 Vaccine Design. *Annu Rev Immunol* **34**, 635-659 (2016).
921 4. P. S. Lee, I. A. Wilson, Structural characterization of viral epitopes recognized by
922 broadly cross-reactive antibodies. *Curr Top Microbiol Immunol* **386**, 323-341 (2015).
923 5. M. S. Gilman *et al.*, Rapid profiling of RSV antibody repertoires from the memory B
924 cells of naturally infected adult donors. *Sci Immunol* **1**, (2016).
925 6. J. S. McLellan, Neutralizing epitopes on the respiratory syncytial virus fusion
926 glycoprotein. *Curr Opin Virol* **11**, 70-75 (2015).

927 7. G. Barba-Spaeth *et al.*, Structural basis of potent Zika-dengue virus antibody cross-
928 neutralization. *Nature* **536**, 48-53 (2016).
929 8. D. F. Robbiani *et al.*, Recurrent Potent Human Neutralizing Antibodies to Zika Virus in
930 Brazil and Mexico. *Cell* **169**, 597-609 e511 (2017).
931 9. M. Xu *et al.*, A potent neutralizing antibody with therapeutic potential against all
932 four serotypes of dengue virus. *NPJ Vaccines* **2**, 2 (2017).
933 10. Z. A. Bornholdt *et al.*, Isolation of potent neutralizing antibodies from a survivor of
934 the 2014 Ebola virus outbreak. *Science* **351**, 1078-1083 (2016).
935 11. S. Chandramouli *et al.*, Structural basis for potent antibody-mediated neutralization
936 of human cytomegalovirus. *Sci Immunol* **2**, (2017).
937 12. K. M. Hastie *et al.*, Structural basis for antibody-mediated neutralization of Lassa
938 virus. *Science* **356**, 923-928 (2017).
939 13. S. C. Harrison, Viral membrane fusion. *Virology* **479-480**, 498-507 (2015).
940 14. D. Corti *et al.*, A neutralizing antibody selected from plasma cells that binds to group
941 1 and group 2 influenza A hemagglutinins. *Science* **333**, 850-856 (2011).
942 15. J. S. McLellan *et al.*, Structure of RSV fusion glycoprotein trimer bound to a
943 prefusion-specific neutralizing antibody. *Science* **340**, 1113-1117 (2013).
944 16. D. R. Burton, Antibodies, viruses and vaccines. *Nat Rev Immunol* **2**, 706-713 (2002).
945 17. D. R. Burton, What Are the Most Powerful Immunogen Design Vaccine Strategies?
946 Reverse Vaccinology 2.0 Shows Great Promise. *Cold Spring Harb Perspect Biol* **9**,
947 (2017).
948 18. J. S. McLellan *et al.*, Structure-based design of a fusion glycoprotein vaccine for
949 respiratory syncytial virus. *Science* **342**, 592-598 (2013).
950 19. A. Impagliazzo *et al.*, A stable trimeric influenza hemagglutinin stem as a broadly
951 protective immunogen. *Science* **349**, 1301-1306 (2015).
952 20. H. M. Yassine *et al.*, Hemagglutinin-stem nanoparticles generate heterosubtypic
953 influenza protection. *Nat Med* **21**, 1065-1070 (2015).
954 21. B. E. Correia *et al.*, Proof of principle for epitope-focused vaccine design. *Nature* **507**,
955 201-206 (2014).
956 22. B. B. Finlay, G. McFadden, Anti-immunology: evasion of the host immune system by
957 bacterial and viral pathogens. *Cell* **124**, 767-782 (2006).
958 23. S. F. Andrews *et al.*, Immune history profoundly affects broadly protective B cell
959 responses to influenza. *Sci Transl Med* **7**, 316ra192 (2015).
960 24. D. Angeletti *et al.*, Defining B cell immunodominance to viruses. *Nat Immunol* **18**,
961 456-463 (2017).
962 25. V. I. Zarnitsyna *et al.*, Masking of antigenic epitopes by antibodies shapes the
963 humoral immune response to influenza. *Philos Trans R Soc Lond B Biol Sci* **370**,
964 (2015).
965 26. V. I. Zarnitsyna, J. Lavine, A. Ellebedy, R. Ahmed, R. Antia, Multi-epitope Models
966 Explain How Pre-existing Antibodies Affect the Generation of Broadly Protective
967 Responses to Influenza. *PLoS Pathog* **12**, e1005692 (2016).
968 27. G. D. Victora, M. C. Nussenzweig, Germinal centers. *Annu Rev Immunol* **30**, 429-457
969 (2012).
970 28. B. Briney *et al.*, Tailored Immunogens Direct Affinity Maturation toward HIV
971 Neutralizing Antibodies. *Cell* **166**, 1459-1470 e1411 (2016).
972 29. J. G. Jardine *et al.*, HIV-1 VACCINES. Priming a broadly neutralizing antibody response
973 to HIV-1 using a germline-targeting immunogen. *Science* **349**, 156-161 (2015).

974 30. M. Silva *et al.*, Targeted Elimination of Immunodominant B Cells Drives the Germinal
975 Center Reaction toward Subdominant Epitopes. *Cell Rep* **21**, 3672-3680 (2017).
976 31. J. C. Boyington *et al.*, Structure-Based Design of Head-Only Fusion Glycoprotein
977 Immunogens for Respiratory Syncytial Virus. *PLoS One* **11**, e0159709 (2016).
978 32. G. A. Kirchenbaum, D. M. Carter, T. M. Ross, Sequential Infection in Ferrets with
979 Antigenically Distinct Seasonal H1N1 Influenza Viruses Boosts Hemagglutinin Stalk-
980 Specific Antibodies. *J Virol* **90**, 1116-1128 (2016).
981 33. K. Van Reeth *et al.*, Heterologous prime-boost vaccination with H3N2 influenza
982 viruses of swine favors cross-clade antibody responses and protection. *NPJ Vaccines*
983 **2**, (2017).
984 34. C. J. Wei *et al.*, Induction of broadly neutralizing H1N1 influenza antibodies by
985 vaccination. *Science* **329**, 1060-1064 (2010).
986 35. P. L. Herve *et al.*, RSV N-nanorings fused to palivizumab-targeted neutralizing
987 epitope as a nanoparticle RSV vaccine. *Nanomedicine* **13**, 411-420 (2017).
988 36. X. Roux *et al.*, Sub-nucleocapsid nanoparticles: a nasal vaccine against respiratory
989 syncytial virus. *PLoS One* **3**, e1766 (2008).
990 37. R. G. Tawar *et al.*, Crystal structure of a nucleocapsid-like nucleoprotein-RNA
991 complex of respiratory syncytial virus. *Science* **326**, 1279-1283 (2009).
992 38. B. E. Correia *et al.*, Computational protein design using flexible backbone remodeling
993 and resurfacing: case studies in structure-based antigen design. *J Mol Biol* **405**, 284-
994 297 (2011).
995 39. B. Kuhlman, D. Baker, Native protein sequences are close to optimal for their
996 structures. *Proc Natl Acad Sci U S A* **97**, 10383-10388 (2000).
997 40. H. Wu *et al.*, Development of motavizumab, an ultra-potent antibody for the
998 prevention of respiratory syncytial virus infection in the upper and lower respiratory
999 tract. *J Mol Biol* **368**, 652-665 (2007).
1000 41. M. G. Joyce *et al.*, Iterative structure-based improvement of a fusion-glycoprotein
1001 vaccine against RSV. *Nat Struct Mol Biol* **23**, 811-820 (2016).
1002 42. J. L. Xu, M. M. Davis, Diversity in the CDR3 region of V(H) is sufficient for most
1003 antibody specificities. *Immunity* **13**, 37-45 (2000).
1004 43. J. F. Scheid *et al.*, Sequence and structural convergence of broad and potent HIV
1005 antibodies that mimic CD4 binding. *Science* **333**, 1633-1637 (2011).
1006 44. E. Goodwin *et al.*, Infants Infected with Respiratory Syncytial Virus Generate Potent
1007 Neutralizing Antibodies that Lack Somatic Hypermutation. *Immunity* **48**, 339-349
1008 e335 (2018).
1009 45. S. Friedensohn, T. A. Khan, S. T. Reddy, Advanced Methodologies in High-Throughput
1010 Sequencing of Immune Repertoires. *Trends Biotechnol* **35**, 203-214 (2017).
1011 46. N. L. Kallewaard *et al.*, Structure and Function Analysis of an Antibody Recognizing
1012 All Influenza A Subtypes. *Cell* **166**, 596-608 (2016).
1013 47. F. Sesterhenn, J. Bonet, B. E. Correia, Structure-based immunogen design-leading the
1014 way to the new age of precision vaccines. *Curr Opin Struct Biol* **51**, 163-169 (2018).
1015 48. G. Ofek *et al.*, Elicitation of structure-specific antibodies by epitope scaffolds. *Proc*
1016 *Natl Acad Sci U S A* **107**, 17880-17887 (2010).
1017 49. N. Jaberolansar *et al.*, Induction of high titred, non-neutralising antibodies by self-
1018 adjuvanting peptide epitopes derived from the respiratory syncytial virus fusion
1019 protein. *Sci Rep* **7**, 11130 (2017).

1020 50. J. S. McLellan *et al.*, Design and characterization of epitope-scaffold immunogens
1021 that present the motavizumab epitope from respiratory syncytial virus. *J Mol Biol*
1022 **409**, 853-866 (2011).
1023 51. R. K. Abbott *et al.*, Precursor Frequency and Affinity Determine B Cell Competitive
1024 Fitness in Germinal Centers, Tested with Germline-Targeting HIV Vaccine
1025 Immunogens. *Immunity* **48**, 133-146 e136 (2018).
1026 52. B. E. Correia *et al.*, Computational design of epitope-scaffolds allows induction of
1027 antibodies specific for a poorly immunogenic HIV vaccine epitope. *Structure* **18**,
1028 1116-1126 (2010).
1029 53. G. D. Victora, P. C. Wilson, Germinal Center Selection and the Antibody Response to
1030 Influenza. *Cell* **163**, 545-548 (2015).
1031 54. P. Tsui *et al.*, Isolation of a neutralizing human RSV antibody from a dominant, non-
1032 neutralizing immune repertoire by epitope-blocked panning. *Journal of Immunology*
1033 **157**, 772-780 (1996).
1034 55. I. Widjaja *et al.*, Characterization of Epitope-Specific Anti-Respiratory Syncytial Virus
1035 (Anti-RSV) Antibody Responses after Natural Infection and after Vaccination with
1036 Formalin-Inactivated RSV. *J Virol* **90**, 5965-5977 (2016).
1037 56. S. F. Andrews *et al.*, High preexisting serological antibody levels correlate with
1038 diversification of the influenza vaccine response. *J Virol* **89**, 3308-3317 (2015).
1039 57. K. Xu *et al.*, Epitope-based vaccine design yields fusion peptide-directed antibodies
1040 that neutralize diverse strains of HIV-1. *Nat Med* **24**, 857-867 (2018).
1041 58. Y. Li *et al.*, Immune history shapes specificity of pandemic H1N1 influenza antibody
1042 responses. *J Exp Med* **210**, 1493-1500 (2013).
1043 59. D. C. Ekiert *et al.*, A highly conserved neutralizing epitope on group 2 influenza A
1044 viruses. *Science* **333**, 843-850 (2011).
1045 60. D. D. Raymond *et al.*, Conserved epitope on influenza-virus hemagglutinin head
1046 defined by a vaccine-induced antibody. *Proc Natl Acad Sci U S A* **115**, 168-173 (2018).
1047 61. W. Dejnirattisai *et al.*, Dengue virus sero-cross-reactivity drives antibody-dependent
1048 enhancement of infection with zika virus. *Nat Immunol* **17**, 1102-1108 (2016).
1049 62. L. C. Katzelnick *et al.*, Antibody-dependent enhancement of severe dengue disease in
1050 humans. *Science* **358**, 929-932 (2017).
1051 63. A. Chevalier *et al.*, Massively parallel de novo protein design for targeted
1052 therapeutics. *Nature* **550**, 74-79 (2017).
1053 64. F. Sievers *et al.*, Fast, scalable generation of high-quality protein multiple sequence
1054 alignments using Clustal Omega. *Mol Syst Biol* **7**, 539 (2011).
1055 65. N. Castagne *et al.*, Biochemical characterization of the respiratory syncytial virus P-P
1056 and P-N protein complexes and localization of the P protein oligomerization domain.
1057 *J Gen Virol* **85**, 1643-1653 (2004).
1058 66. D. W. Kulp *et al.*, Structure-based design of native-like HIV-1 envelope trimers to
1059 silence non-neutralizing epitopes and eliminate CD4 binding. *Nat Commun* **8**, 1655
1060 (2017).
1061 67. T. A. Khan *et al.*, Accurate and predictive antibody repertoire profiling by molecular
1062 amplification fingerprinting. *Sci Adv* **2**, e1501371 (2016).
1063 68. S. Friedensohn *et al.*, Synthetic Standards Combined With Error and Bias Correction
1064 Improve the Accuracy and Quantitative Resolution of Antibody Repertoire
1065 Sequencing in Human Naive and Memory B Cells. *Front Immunol* **9**, 1401 (2018).

69. Z. Gu, L. Gu, R. Eils, M. Schlesner, B. Brors, circlize Implements and enhances circular visualization in R. *Bioinformatics* **30**, 2811-2812 (2014).
70. J. Ou, S. A. Wolfe, M. H. Brodsky, L. J. Zhu, motifStack for the analysis of transcription factor binding site evolution. *Nat Methods* **15**, 8-9 (2018).